Magnetization reversal and anisotropic magnetoresistance behavior in bicomponent antidot nanostructures

D. Tripathy,[1] P. Vavassori,[2,3] J. M. Porro,[2] A. O. Adeyeye,[1,a)] and N. Singh[4]
[1]*Department of Electrical and Computer Engineering, Information Storage Materials Laboratory, National University of Singapore, Singapore 117576*
[2]*CIC nanoGUNE Consolider, Tolosa Hiribidea, 76, E-20018 Donostia-San Sebastian, Spain*
[3]*Dipartimento di Fisica, CNR-INFM S3, CNISM, Universita' di Ferrara, I-44100 Ferrara, Italy*
[4]*A*Star Institute of Microelectronics, 11 Science Park Road, Singapore Science Park II, Singapore 117685*

(Received 16 April 2010; accepted 8 July 2010; published online 30 July 2010)

We report on the magnetic properties and anisotropic magnetoresistance behavior of engineered bicomponent array of "holes" with alternating diameters embedded in a continuous permalloy film. We observed that the magnetization reversal is significantly altered when compared to a homogeneous array of antidots, and exhibits strong dependence on the permalloy thickness. Our results demonstrate that the use of two antidot sublattices greatly enhances the parameters available for engineering the behavior of antidot nanostructures. © *2010 American Institute of Physics*. [doi:10.1063/1.3474802]

Advancements in lithography tools for fabricating nanostructures with precisely controlled dimensions and geometry have led to a steady miniaturization in the physical size of magnetic elements in recent years, and have concurrently stimulated tremendous interest in magnetic nanostructures for practical applications in high density data storage.[1] In this regard, antidot nanostructures, which consist of a mesh of nonmagnetic "holes" embedded in a continuous magnetic film,[2] provide an effective method to engineer magnetic properties in a controllable manner, and have been proposed as a candidate for ultra high density storage media with characteristics that encompass improved thermal stability and circumventing the superparamagnetic limit. These "holes" alter demagnetizing fields and act as domain wall pinning sites that hinder the propagation of domain walls, thus resulting in an enhanced coercivity as compared to continuous films, and also provide an effective technique for engineering the magnetic anisotropy. Due to their inherent fundamental and technological importance, it is imperative to have control over the switching mechanism in antidot nanostructures for tailor-made properties.

One of the techniques which has been employed to influence the switching mechanisms during magnetization reversal is to vary the antidot shape (square, circular, elliptical), size, and interelement spacing.[3–7] Moreover, it has also been demonstrated that by carefully adjusting the symmetry order of the antidot lattice, local magnetic anisotropy distributions can be altered to conform to the lattice symmetry, such that reversal process takes place through a collective and periodic domain nucleation and expansion process.[8] Another perspective which has received much attention involves the use of multilayer films, and has been employed to realize a wide gamut of phenomena that include perpendicular anisotropy,[9] asymmetric reversal due to exchange bias,[10,11] and also varying the reversal mechanism as a consequence of interlayer coupling in spin valve antidot nanostructures.[12] While most of the reported work in literature on controlling the magnetization reversal has focused on homogeneous arrays of antidots, the possibility of utilizing bicomponent nanostructures in which nearest neighbor antidots are of alternating dimensions is yet to be explored.

In this paper, we report on tailoring the magnetization reversal in bicomponent antidot nanostructures by patterning neighboring antidots with alternate dimensions. We demonstrate that the use of two antidot sublattices greatly enhances the parameters available for engineering the behavior of antidot nanostructures.

Bicomponent antidot nanostructures with alternating diameters were fabricated over a large area (4×4 mm^2) on commercially available Si substrates using deep ultraviolet (DUV) lithography at 248 nm exposing wavelength, followed by e-beam evaporation of permalloy ($Ni_{80}Fe_{20}$) films of varying thickness t and ultrasonic assisted lift-off in OK73 resist thinner. Details of the fabrication process are described elsewhere.[1] Figure 1 shows the scanning electron microscopy (SEM) image of the final structure consisting of bicomponent antidot nanostructures with alternating diameters D_1

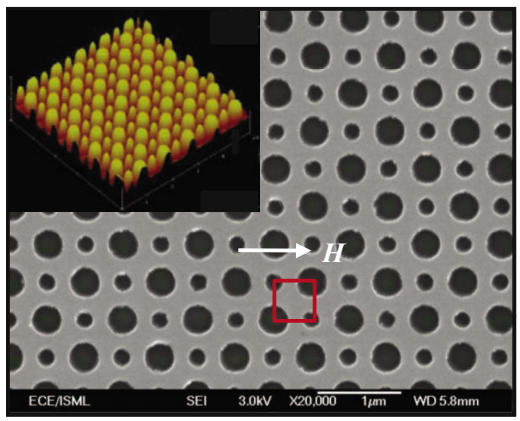

FIG. 1. (Color online) SEM image of inhomogeneous antidot arrays consisting of antidots with alternating diameters D_1=350 nm, D_2=200 nm, and center-to-center spacing between these two adjacent antidots fixed at λ=450 nm. The inset shows the atomic force microscopy resist profile after exposure and development.

a)Author to whom correspondence should be addressed. Electronic mail: eleaao@nus.edu.sg.

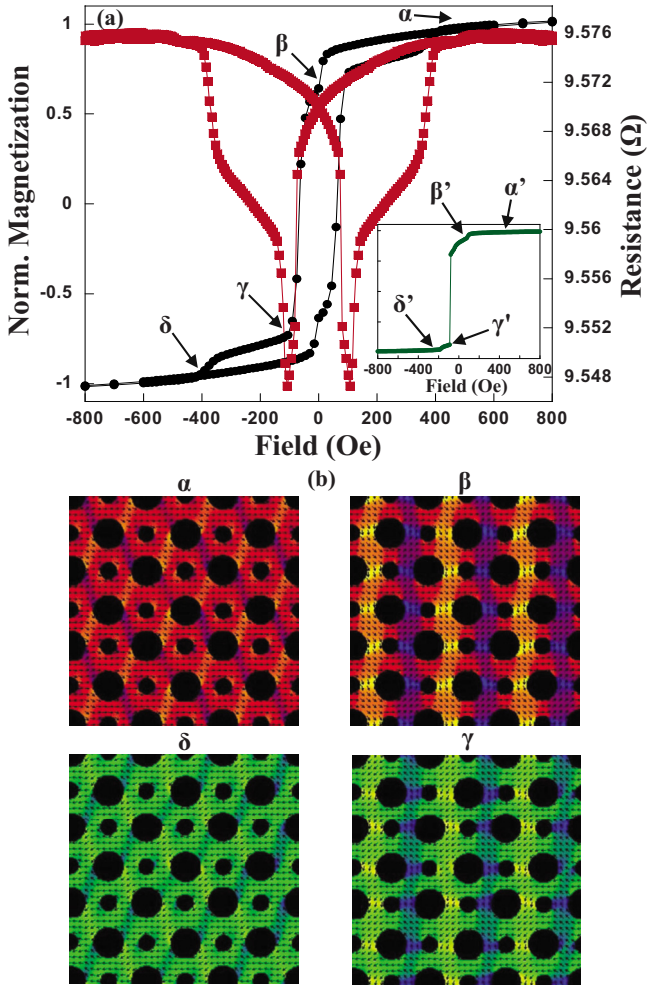

FIG. 2. (Color online) (a) In-plane magnetization curve and the corresponding LMR curve for the antidot nanostructures measured at room temperature for $t=80$ nm with inset showing the simulated magnetization curve, and (b) magnetization states obtained from LLG simulation at varying external magnetic fields.

$=350$ nm and $D_2=200$ nm, and center-to-center spacing between these two adjacent antidots fixed at $\lambda=450$ nm. For all the results shown in this work, the orientation of the external magnetic field H as illustrated schematically in Fig. 1 is along the edge of the square unit cell. Detailed insight into the magnetization reversal mechanism in the antidots was facilitated by micromagnetic modeling which was performed using LLG Micromagnetic software.[13] We have utilized three-dimensional modeling using the SEM image as a bitmap with periodic boundary conditions. Standard parameters were used to characterize the properties of $Ni_{80}Fe_{20}$ (exchange constant $A=13\times10^{-12}$ J m^{-1}, saturation moment $M_s=800$ kAm^{-1}, and anisotropy constant $K_U=0$).

Figure 2 shows the representative in-plane magnetization curve and the corresponding anisotropic magnetoresistance (AMR) curves in the longitudinal geometry (field parallel to current density) at room temperature for $t=80$ nm, in conjunction with the magnetization states obtained from LLG simulation at various stages of reversal. The simulated magnetization curve is shown as an inset in Fig. 2(a). Experimentally, we observed that when compared to homogeneous circular antidot nanostructures of comparable dimensions and film composition,[5] the magnetization reversal mechanism is markedly modified due to the alternating dimensions of adjacent antidots. The reversal occurs via *three* characteristic switching fields which are clearly evident in both the magnetization and the longitudinal magnetoresistance (LMR) curves. The experimental results are in qualitative agreement with the micromagnetic modeling, although it is important to note that the simulated magnetization curve exhibits sharper transitions and different switching fields. This is expected since the simulation only considers the response of a limited number of unit cells with periodic boundaries due to computation limitations, and does not take into account the defect distribution in the actual sample.

At positive saturation field, all the spins in the antidot structure are aligned along the field direction. As the external magnetic field is progressively reduced from the saturation, surface magnetic charges at the boundary between the $Ni_{80}Fe_{20}$ layer and the antidot edges lead to the formation of domains via demagnetizing fields. Magnetization state α in Fig. 2(b) shows one such highly ordered domain configuration. The corresponding position on the simulated curve is indicated as α'. It is important to note that unlike homogeneous antidot nanostructures where four wedge shaped domains connect each antidot to its nearest neighbor at each end,[7,14] the domain patterns for our bicomponent antidots are considerably altered. We observed that the wedge shaped domains now connect only the larger antidots ($D=350$ nm) to their respective closest neighbors of identical dimension instead of the nearest neighbor smaller antidots ($D=200$ nm), and the spins are oriented at $\pm45°$ to the field direction. While the nucleation of wedge shaped domains around the smaller antidots is also discernible, they are unable to stretch out and connect to their counterpart antidots of identical size. The domain configuration may be ascribed to the additional anisotropy that has been induced in the bicomponent antidot nanostructures. Moreover, the relaxation of spins with decreasing field also causes the spins to deviate from the local current density thereby resulting in the smooth reduction in resistance in the LMR curve.

With further reduction in magnetic field, we observed that the magnetization continues to decrease gradually until there is a drop of $\sim15\%$ near remanence due to the formation of the domain pattern shown in state β. Compared to state α, it can be seen that the wedge shaped domains from each of the smaller antidots have now coalesced with the adjacent larger domains, thereby resulting in a reduction in the area of domains that are parallel to the applied field direction. This is accompanied by rotation of the wedge shaped domains between the larger antidots in alternate rows by $\pm90°$. Furthermore, we also observe that small vertical domains now exist between each pair of large/small antidots in every row of the structure, and are alternately oriented at $\pm90°$ to the field direction. The jump in magnetization is also accompanied by a change in slope of the LMR curve due to the increasing angle between magnetization and current density. When the field is now increased in the opposite direction, magnetization as well as resistance decreases continuously due to the rotation of domains until a critical field of $H=-60$ Oe is reached upon which irreversible switching is activated. The steep change in magnetization and resistance persists until the intermediate domain configuration shown in state γ is formed. This state represents a transitional configuration, where the irregular domains have undergone a 180° magnetization rotation from state β, while the

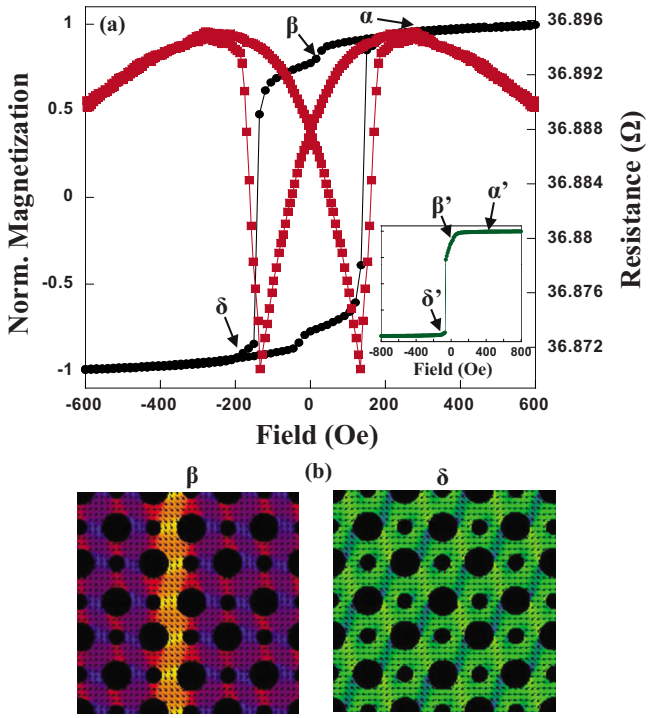

FIG. 3. (Color online) (a) In-plane magnetization curve and the corresponding LMR curve for the antidot nanostructures measured at room temperature for $t=30$ nm with inset showing the simulated magnetization curve, and (b) magnetization states obtained from LLG simulation.

wedge shaped domains between the larger antidots have rotated further by 90°. The smaller vertical domains from state β, however, retain their previous orientation. As the reverse field is further increased, the change in both magnetization and resistance is again gradual and corresponds to the transition of the domains to the stable magnetic state shown as δ, and reflects the condition when all the wedge shaped domains between the larger antidots have completed a 180° rotation from their original orientation in state α and the spins are now oriented at $\pm 135°$ to the field direction. Further increase in reverse field leads to the final switching and signals the completion of magnetization reversal in the antidot nanostructures as all the spins gradually align along the reverse field direction.

To further understand the magnetization reversal process, we have also characterized the bicomponent antidot nanostructures for $t=30$ nm. Figure 3(a) clearly shows that the reversal process is strongly dependent on the $Ni_{80}Fe_{20}$ layer thickness. The magnetization reversal now occurs via *two* distinct switching processes, thereby suggesting that one or more domain configurations that existed for $t=80$ nm are not energetically favorable for $t=30$ nm. To strengthen this argument, relevant magnetization states obtained from LLG simulation were captured and are shown in Fig. 3(b). The initial reversal process as the field is reduced from positive saturation is similar to $t=80$ nm with the formation of ordered domain patterns with wedge shaped domains connecting the larger antidots [state α in Fig. 2(b)]. However, the first jump in magnetization is not as abrupt (~5%), while state β closely resembles its counterpart for $t=80$ nm, except for the fact that the small vertical domains between the large/small antidots are oriented at $-90°$ to the field direction only for one column. As the field is now increased further in the reverse direction, magnetization as well as resistance decrease continuously due to the rotation of domains until the critical field for irreversible switching is reached at $H=-140$ Oe, which is also higher than the irreversible switching field obtained for $t=80$ nm. With further increase in reverse field, magnetization decreases sharply till the ordered domain configuration, with both the wedge shaped domains connecting larger antidots and irregular shaped domains between each large/small having undergone a 180° magnetization rotation, is directly formed, as shown in δ. Hence, in sharp contrast to $t=80$ nm, an intermediate state similar to γ in Fig. 2(b) does not form, and the magnetization reversal taking place only via two distinct switching processes ($\alpha \rightarrow \beta \rightarrow \delta$).

In summary, we have investigated the magnetization reversal behavior in bicomponent antidot nanostructures consisting of adjacent antidots with alternate dimensions. We observed that the reversal mechanism is markedly modified as a consequence of domain configurations that exist due to the different "hole" dimensions of adjacent antidots. Our results conclusively demonstrate a suitable technique with increased capability for tailoring the magnetic properties of antidot nanostructures.

This work was supported by the Agency of Science, Technology and Research (A*Star), Singapore under Grant No. 062-101-0022 and National Research Foundation (NRF), Singapore under Grant No. NRFG-CRP 2007-05. P.V. acknowledges funding from the Department of Industry, Trade, and Tourism of the Basque Government, the Provincial Council Gipuzkoa under the ETORTEK Program (Project No. IE06-172), the Spanish MICINN (Project No. CSD2006-53), and the EU VII Framework Programme (Grant Agreement No. PIEF-GA-2008-220166). The authors would like to thank S. Jain for her assistance in LLG simulation.

[1] A. O. Adeyeye and N. Singh, J. Phys. D: Appl. Phys. **41**, 153001 (2008).
[2] A. O. Adeyeye, J. A. C. Bland, and C. Daboo, Appl. Phys. Lett. **70**, 3164 (1997).
[3] I. Guedes, M. Grimsditch, V. Metlushko, P. Vavassori, R. Camley, B. Ilic, P. Neuzil, and R. Kumar, Phys. Rev. B **66**, 014434 (2002).
[4] A. Y. Toporov, R. M. Langford, and A. K. Petford-Long, Appl. Phys. Lett. **77**, 3063 (2000).
[5] C. C. Wang, A. O. Adeyeye, N. Singh, Y. S. Huang, and Y. H. Wu, Phys. Rev. B **72**, 174426 (2005).
[6] U. Welp, V. K. Vlasko-Vlasov, G. W. Crabtree, C. Thompson, V. Metlushko, and B. Ilic, Appl. Phys. Lett. **79**, 1315 (2001).
[7] C. T. Yu, H. Jiang, L. Shen, P. J. Flanders, and G. J. Mankey, J. Appl. Phys. **87**, 6322 (2000).
[8] P. Vavassori, G. Gubbiotti, G. Zangari, C. T. Yu, H. Yin, H. Jiang, and G. J. Mankey, J. Appl. Phys. **91**, 7992 (2002).
[9] M. T. Rahman, N. N. Shams, C. H. Lai, J. Fidler, and D. Suess, Phys. Rev. B **81**, 014418 (2010).
[10] D. Tripathy and A. O. Adeyeye, Phys. Rev. B **79**, 064413 (2009).
[11] D. Tripathy, A. O. Adeyeye, and N. Singh, Appl. Phys. Lett. **93**, 022502 (2008).
[12] C. C. Wang, A. O. Adeyeye, and N. Singh, Appl. Phys. Lett. **88**, 222506 (2006).
[13] M. R. Scheinfein, LLG Micromagnetics Simulator, http://llgmicro.home.mindspring.com.
[14] G. Ctistis, E. Papaioannou, P. Patoka, J. Gutek, P. Fumagalli, and M. Giersig, Nano Lett. **9**, 1 (2009).